Effective radiative properties of bounded cascade nonabsorbing clouds: Definition of the equivalent homogeneous cloud approximation

Frédéric Szczap, Harumi Isaka, Marcel Saute, Bernard Guillemet, Andrey Ioltukhovski

JOURNAL OF GEOPHYSICAL RESEARCH, VOL. 105, NO. D16, PAGES 20,617–20,633, AUGUST 27, 2000

Effective radiative properties of bounded cascade nonabsorbing clouds: Definition of the equivalent homogeneous cloud approximation

Frédéric Szczap, Harumi Isaka, Marcel Saute, and Bernard Guillemet

Laboratoire de Météorologie Physique, Université Blaise Pascal, Aubière, France

Andrey Ioltukhovski

Keldish Institute of Applied Mathematics, Moscow

Abstract. In the present study we investigated the radiative properties of inhomogeneous nonabsorbing clouds under the Equivalent plane-parallel Homogeneous Cloud Approximation (EHCA), by using the one-dimensional (1-D) bounded cascade inhomogeneous clouds. The effective optical depth was defined under the EHCA by requiring the identity of the radiant flux components of the radiation budget between the inhomogeneous clouds and their equivalent homogeneous counterparts. Such requirement provides a rational framework to define the effective optical depth of the inhomogeneous nonabsorbing clouds. We analyzed the dependency of the effective optical depth on the horizontal scale of averaging and solar incidence angle and specified the conditions under which an inhomogeneous cloud segment could be treated as a plane-parallel homogeneous cloud. A parameterization of the effective optical depth was proposed as a function of the mean optical depth and a relative cloud inhomogeneity parameter. Finally, we compared the EHCA with the effective thickness approximation, both based on the definition of the effective optical depth, and discussed the difference between their respective effective optical depths.

1. Introduction

Clouds exhibit fluctuations of microphysical characteristics at different spatial scales. How this spatial inhomogeneity of cloud properties affects the radiative transfer is one of the major issues of the atmospheric radiation theory. Many physicists have recently investigated the problem of cloud inhomogeneity with renewed interest. Some have attempted to evaluate its effect on radiant flux components of the cloud radiation budget [*Barker*, 1992, 1996a, b; *Barker et al.*, 1996; *Cahalan et al.*, 1994a; *Marshak et al.*, 1995b, 1998; *Borde and Isaka*, 1996; *Chambers et al.*, 1997; *Oreopoulos and Davies*, 1998a, b; *Oreopoulos and Barker*, 1999]. Others have analyzed the statistical characteristics of the radiation fields of natural clouds by using Landsat and/or AVHRR images [*Barker and Davies*, 1992; *Davis et al.*, 1997; *Marshak et al.*, 1998], or in situ measurements [*Cahalan and Snider*, 1989; *Davis et al.*, 1996, 1999]. In these studies the emphasis was put on the interaction of the radiative transfer process with the "sub-cloud scale" fluctuations of microphysical properties as well as on its scaling and auto-similarity properties. The spatial scales of the cloud inhomogeneity considered in these studies differ significantly from those considered in the earlier studies on the broken cloud fields, in which the radiative interaction was considered between isolated clouds with simple geometrical shapes [*McKee and Cox*, 1974; *Aida*, 1977; *Davies*, 1978; *Schmetz*, 1984; *Bréon*, 1992; *Barker*, 1994; *Zuev and Titov*, 1995].

Another issue emphasized in these studies is the easy and fast calculation of the radiant flux components of the radiation budget of the inhomogeneous clouds in general circulations models (GCMs). We can distinguish schematically two approaches to this calculation: the independent pixel approximation (IPA) proposed by *Cahalan et al.* [1994b] and its variants, and the Effective Thickness Approximation (ETA) also proposed by Cahalan et al. [1994a] and its variants. These two approaches are sometimes confused and considered as equivalent. However, there is a significant conceptual difference between the ETA and the IPA, although the ETA was initially introduced through the area averaging of the IPA radiant fluxes. It is revealing that the gamma IPA [*Barker*, 1996b], mentioned below, did not invoke an effective optical depth, which suggests that the concept of effective optical depth and effective radiative properties, in general, is not an inherent element of the IPA.

Paper number 2000JD900146.
0148-0227/00/2000JD900146$09.00

Cahalan et al. [1994b] showed that the IPA could provide an "accurate" area-averaged reflectance of the bounded cascade inhomogeneous clouds at mesoscale. Its extension to the cloud pixels or cloud segments was done as the nonlocal independent pixel approximation (NIPA) by *Marshak et al.* [1995b, 1998] and as the gamma IPA by *Barker* [1996b] and *Barker et al.* [1996]. The applicability of the gamma IPA depends on that of the IPA, since it is proposed as a computer-efficient approximation to the IPA [*Barker*, 1996]. The IPA and its variants rely on the "error-smoothing" effect of area averaging to calculate the area-averaged radiant fluxes of the inhomogeneous clouds. Accordingly, the IPA is not necessarily restricted to the bounded cascade type of inhomogeneous clouds. Furthermore, since the averaging is a simple linear operation, the IPA assumes implicitly that the interaction of the radiative transfer process with the cloud inhomogeneity does not exhibit a large nonlinear effect when the radiant fluxes are averaged over an area large enough to neglect the contribution of the net horizontal photon transport.

On the other hand, the ETA and its variants (the equivalent homogeneous cloud approximation we proposed below can be considered as one of them) aimed to treat the inhomogeneous clouds under the plane-parallel homogeneous (PPH) cloud assumption. The effective radiative parameters are defined by requiring the identity of radiant flux components between the inhomogeneous cloud and their equivalent homogeneous counterparts. The key element of this approach is the functional relations between the effective radiative parameters and the mean radiative and structural parameters of the inhomogeneous clouds. Consequently, the ETA and its variants are not to be considered only as a method of radiant flux calculation as the IPA but a method to analyze the nonlinear effect of the "radiative transfer-cloud inhomogeneity" interaction, which is embodied by the above functional relations themselves. When the ETA is used to calculate the radiant flux components, the performance of the ETA should differ from that of the IPA according to the importance of the nonlinear effect in the "radiative transfer-cloud inhomogeneity" interaction.

A fractal or multifractal cloud could be treated under the PPH cloud assumption and its effective optical depth be expressed as a function of the cloud inhomogeneity [*Cahalan et al.*, 1994b; *Borde and Isaka*, 1996]. However, in these studies the cloud inhomogeneity was represented by fractal parameters of the cascade processes used for the inhomogeneous-cloud generation. Therefore their effective optical depths are applicable only to the scale of the entire cloud domain but not to the scale of a cloud segment. Furthermore, such fractal parameters are only relevant to the inhomogeneous clouds generated with those specific cascade processes (bounded cascade in the work of Cahalan et al. and lognormal cascade in the work of Borde and Isaka) but not to the clouds generated with other cloud-generation processes. Hence there is a need to investigate how the ETA approach can be extended to the cloud segments, but also to define pertinent parameters to represent the nonlinear effect of the cloud inhomogeneity at the scale of cloud segments.

In most of the above studies, the emphasis was put only on the reflectance or albedo of the inhomogeneous clouds and its approximation. However, for GCM applications we need to consider not only the energy reflected from the clouds but also the other radiant flux components (absorptance and transmittance) of the radiation budget. For example, we have to compute, in some case, the radiation budget of inhomogeneous clouds with highly reflecting underlying earth surface. Doing so under the plane-parallel homogeneous cloud assumption requires the precise definition of an equivalent plane-parallel homogeneous cloud and its effective radiative properties within an adequate theoretical framework. From this point of view, the EHCA can be considered as an attempt to develop the ETA approach within a more formal framework and then to extend it to the inhomogeneous absorbing clouds [*Szczap et al.*, this issue].

The retrieval of cloud parameters from remotely sensed multispectral radiometric data is another field of interest in which we have to consider the cloud inhomogeneity. The actual cloud parameter retrieval assumes that a plane-parallel homogeneous cloud model is valid at the scale of one satellite image pixel [*Nakajima and King*, 1988, 1990; *Twomey and Cocks*, 1989; *Wetzel and Vonder Haar*, 1991]. This implies that when the optical depth is retrieved, it is effective and not average optical depth. To correct the effect of the subpixel scale cloud inhomogeneity on the retrieved optical depth requires the knowledge of the functional relation between the effective optical depth and the mean parameters (mean optical depth, subpixel scale cloud inhomogeneity). This would be within the scope of the ETA and its variants (T. Faure et al., Neural network retrieval of cloud parameters of inhomogeneous and fractional clouds from multispectral reflectance data: feasibility study, submitted to *Remote Sensing of Environment*, 1999c (hereinafter referred to as F99c)) but not within the scope of the IPA and its variants. For example, *Marshak et al.* [1995b] attempted to retrieve the optical depth of inhomogeneous clouds directly from high-resolution radiometric data under the NIPA. However, this approach as such is not applicable to moderate resolution radiometric data (advanced very high resolution radiometer (AVHRR), Moderate-Resolusion Imaging Spectroradiometer (MODIS), global imager on adeos 2) *(GLI)*, because it cannot take into account the subpixel scale cloud inhomogeneity. This problem in itself differs from the one investigated at multipixels scale by *Barker et al.* [1996] and *Davis et al.* [1997].

The purposes of this study are to answer the different questions asked above: (1) to define the effective optical depth under the equivalent homogeneous plane-

parallel cloud approximation (EHCA) with the requirement of identity of the radiant flux components between the inhomogeneous clouds and their homogeneous counterparts; (2) to specify the conditions under which an inhomogeneous cloud segment can be treated under the plane-parallel homogeneous cloud assumption; (3) to analyze the dependency of the effective optical depth on the horizontal averaging scale and solar incidence angle; and (4) to derive an empirical equation relating the effective optical depth to the local mean optical depth and a relative cloud inhomogeneity parameter. Finally, we discuss the basic difference between the EHCA and the ETA [*Cahalan et al.*, 1994a, b]. This study is based on the use of (1-D) bounded cascade inhomogeneous cloud as in most of the studies mentioned above, excluding the broken cloud fields from our scope. We discussed, elsewhere, the extension of the EHCA to the inhomogeneous absorbing clouds [*Szczap et al.*, this issue] and 2-D inhomogeneous clouds [*Szczap et al.*, 2000]. The application of the EHCA to the cloud parameter retrieval is discussed by F99c.

2. Conditions of Simulation

2.1. Monte Carlo Radiative Transfer Code

The Monte Carlo (MC) method is the simplest numerical tool to compute the radiative transfer in an arbitrarily inhomogeneous medium. Assuming the extinction coefficient and single-scattering albedo independent of the incident direction, we can write the radiative transfer equation

$$\vec{\Omega}\cdot\vec{\nabla}I(\vec{r},\vec{\Omega}) + \sigma(\vec{r})I(\vec{r},\vec{\Omega}) = \omega(\vec{r})\sigma(\vec{r})\int_{4\pi}\gamma(\vec{\Omega},\vec{\Omega}')I(\vec{r},\vec{\Omega}')d\vec{\Omega}', \quad (1)$$

where $I(\vec{r},\vec{\Omega})$ designates the radiant intensity along a direction vector at a point $\vec{r}$, $\sigma(\vec{r})$ and $\omega(\vec{r})$ are the extinction coefficient and the single-scattering albedo at point $\vec{r}$; $\gamma(\vec{\Omega},\vec{\Omega}')$ is the volume scattering phase function from an incident direction $\vec{\Omega}'$ to another direction $\vec{\Omega}$. The replacement of $\vec{r}$ with $\alpha\vec{r}$ yields

$$\vec{\Omega}\cdot\vec{\nabla}\ I(\alpha\vec{r},\vec{\Omega}) + \alpha\sigma(\alpha\vec{r})I(\alpha\vec{r},\vec{\Omega}) = \omega(\alpha\vec{r})\alpha\sigma(\alpha\vec{r})\int_{4\pi}\gamma(\vec{\Omega},\vec{\Omega}')I(\alpha\vec{r},\vec{\Omega}')d\vec{\Omega}', \quad (2)$$

where α is a similarity coefficient. Because of this identity of radiation fields for homothetic media, we can use a fixed cloud domain for our simulation of radiative transfer in inhomogeneous clouds without much loss of generality. In the maximal cross-section method [*Marchuk et al.*, 1980; *Marshak et al.*, 1995a], equation (1) is transformed into

$$\vec{\Omega}.\vec{\nabla}I(\vec{r},\vec{\Omega}) + \sigma_{max}(\vec{r})I(\vec{r},\vec{\Omega}) = \sigma_{max}\int_{4\pi}[\frac{\sigma(\vec{r})}{\sigma_{max}}\omega\gamma(\vec{\Omega}.\vec{\Omega}') + (1-\frac{\sigma(\vec{r})}{\sigma_{max}})\delta(\vec{\Omega}-\vec{\Omega}')]I(\vec{r},\vec{\Omega}')d\vec{\Omega}', \quad (3)$$

where σ_{max} represents the maximum extinction coefficient in the cloud domain. We used the MC code [*Marshak et al.*, 1995a] for both the homogeneous and the inhomogeneous clouds.

2.2. Generation of Bounded Cascade Inhomogeneous Clouds

For MC simulation we have to generate inhomogeneous clouds with prescribed characteristics of cloud inhomogeneity. Fractal and multifractal analyses were recently used to study the scaling and autosimilarity properties of natural clouds and cloud fields [*Lovejoy*, 1982; *Cahalan*, 1989; *Duroure and Guillemet*, 1990; *Cahalan et al.*, 1994a; *Marshak et al.*, 1995b], but also to simulate synthetic inhomogeneous clouds [*Scherzter and Lovejoy*, 1991; *Davis et al.*, 1994]. A multifractal medium can be generated with the lognormal cascade process [*Monin and Yaglom*, 1975], but it tends to produce "unrealistic" intermittent fluctuations of cloud properties. *Cahalan et al.* [1994a] and *Marshak et al.* [1994] proposed a bounded cascade process in which the multiplicative factor W_n varies with the scale $r_n = \frac{L}{2^n}$ at step n like

$$W_n = 1 \pm \frac{1-2p}{2^{(n-1)H}}, \quad (4)$$

where the plus and minus signs occur with equal probability, and H and $2p$ are usual fractal parameters of the bounded cascade process [*Marshak*, 1994]. The bounded cascade model remedies the -1 limitation of the spectral slope that constitutes a major flaw of the lognormal process. Furthermore, the bounded cascade inhomogeneous clouds are considered as a fair approximation to 1-D horizontal fluctuations of liquid water path within low-level stratiform clouds [*Cahalan et al.*, 1994a].

The model parameters H and $2p$ were set equal to 0.25 and 0.50; then, the power spectrum of the optical depth fluctuations has a theoretical spectral slope of -1.5. The cloud domain is of 12.8 km in the horizontal and 0.3 km in the vertical. It is composed of 256 elementary "bar" cloud pixels, each one of which is 50 m wide in the x direction and infinite in the y direction. The number of cascades and the horizontal extent of cloud domain are chosen in such a way that the inhomogeneous clouds be characterized by a moderate to large standard deviation of fluctuations in the optical depth when averaged over a scale of kilometers. The cloud domain is repeated horizontally to obtain an inhomogeneous cloud of infinite horizontal extent.

The optical depth, hence the liquid water content, is assumed to be vertically uniform in each cloud pixel; the fluctuations of the optical depth correspond to the fluctuations of the droplet concentration. The droplet size distribution is of the $C1$ type, and the volume-scattering phase function is computed for monochromatic light of 0.55 μm [*Garcia and Siewert*, 1985]. The asymmetry factor ($g = 0.848$ at 0.55 μm) does not change signifi-

cantly for droplet size distributions usually observed in low-level stratiform clouds [*Davies et al.*, 1984]. On the other hand, *Borde and Isaka* [1996] showed that its effect on the effective optical depth is linear, and it should remain small in our case.

We generated independently an inhomogeneous cloud for each MC simulation. For a given solar zenithal angle θ_0, MC simulation was carried out for different values of the mean-cloud optical depth $\bar{\tau}$ (from 1 to 60); we sometimes qualify a mean optical depth as "cloud - mean" to stress that the mean is taken over the entire cloud domain (12.8 km) and not over a cloud segment. For each $\bar{\tau}$, we generated three independent clouds by varying the seed of the cascade process and realized MC simulation for each one of them. The exception to this is a series of special simulations discussed in the subsection 3.1.3.

MC simulations were done, by using 3×10^7 photons (approximately 1.2×10^5 photons/cloud pixel). We computed the reflectance and transmittance for each cloud pixel and the area-averaged reflectance and transmittance over cloud segments of L. The MC method has an intrinsic statistical error, which decreases with the increasing number of photons. When the average reflectance and transmittance were computed over a segment 0.8 km wide, the relative error remains less than about 5×10^{-3} (Appendix A). Since $L = 0.8$ km is the smallest scale of averaging in this study, this value constitutes the upper bound of the relative error in the reflectance and transmittance reported below.

3. Analysis of Monte Carlo Simulations

The plan of the present analysis is as follows. In subsection 3.1, we study how the horizontal averaging scale affects the effective optical depth of inhomogeneous clouds and discuss the conditions under which the plane-parallel homogeneous (PPH) cloud model can be applied to the bounded cascade inhomogeneous clouds. In subsection 3.2, we establish a relation between the effective optical depth, the mean optical depth, and cloud inhomogeneity parameter. Finally, the difference between the EHCA and ETA is discussed in subsection 3.3. When an inhomogeneous cloud is generated with a cascade process, the first few steps of the cascade condition the fluctuations at large horizontal scale. Accordingly, these fluctuations cannot be considered "completely random" because of a very limited number of possible configurations [*Monin and Yaglom*, 1975]. Hence, we randomized the cloud segment locations within the entire cloud domain to eliminate eventual systematic bias that could result from this limited configuration number.

3.1. Equivalent Homogeneous Cloud, Effective Optical Depth and Horizontal Averaging Scale

3.1.1. Equivalent homogeneous cloud approximation. Let us define a PPH cloud equivalent to an arbitrary inhomogeneous cloud by requiring that it has either the same reflectance or transmittance as that of the inhomogeneous cloud. The reflectance and transmittance of a PPH cloud are shown in Figure 1 as a function of the optical depth for a given solar incidence angle. The effective optical depth can be defined from either the reflectance τ^R_{eff} or transmittance τ^T_{eff} according to the following relations:

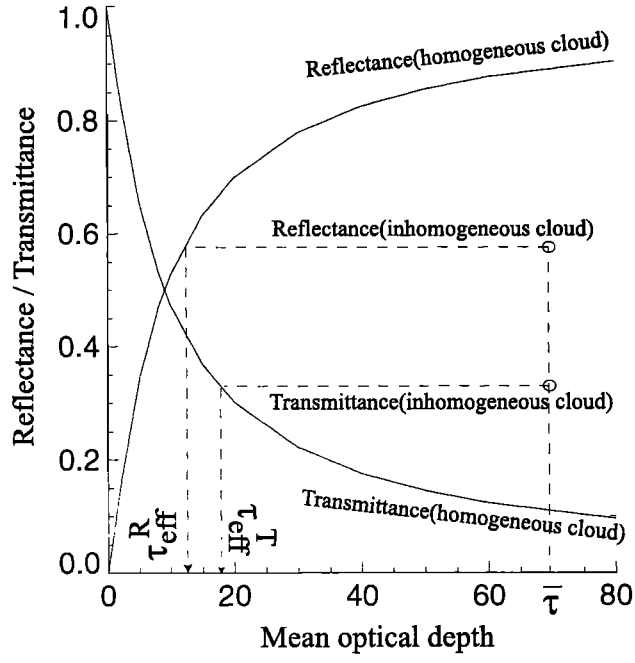

Figure 1. Schematic representation of the method used to determine τ^R_{eff} and τ^T_{eff} of an inhomogeneous cloud segment from its "measured" reflectance and transmittance.

$$R_{\text{hom}}\left(\tau^R_{\text{eff}}, \theta_0\right) = R_{\text{inhom}}\left(\bar{\tau}, \theta_0\right) \quad \text{or}$$
$$T_{\text{hom}}\left(\tau^T_{\text{eff}}, \theta_0\right) = T_{\text{inhom}}\left(\bar{\tau}, \theta_0\right), \tag{5}$$

$$\tau^R_{\text{eff}} = R^{-1}_{\text{hom}}\left[R_{\text{inhom}}\left(\bar{\tau}, \theta_0\right), \theta_0\right] \quad \text{or}$$
$$\tau^T_{\text{eff}} = T^{-1}_{\text{hom}}\left[T_{\text{inhom}}\left(\bar{\tau}, \theta_0\right), \theta_0\right], \tag{6}$$

where $\bar{\tau}$ designates the cloud-mean optical depth of an inhomogeneous cloud, R_{hom} and T_{hom}, respectively, the reflectance and transmittance of its equivalent homogeneous cloud.

The equivalent homogeneous cloud defined above does not have necessarily the "same reflectance and same transmittance" as that of the original inhomogeneous cloud, because its τ^R_{eff} and τ^T_{eff} do not necessarily agree with each other. The radiation budget of an inhomogeneous cloud or cloud segment can be treated under the PPH cloud assumption, only when τ^R_{eff} and τ^T_{eff} are identical within a prescribed error. The requirement of the identity between these two effective optical depths is the essential element of the EHCA; the effective optical depths defined in *Cahalan et al.* [1994b] or *Borde and Isaka* [1996] are not based on such requirement. In the subsequent sections, we will examine the effect of

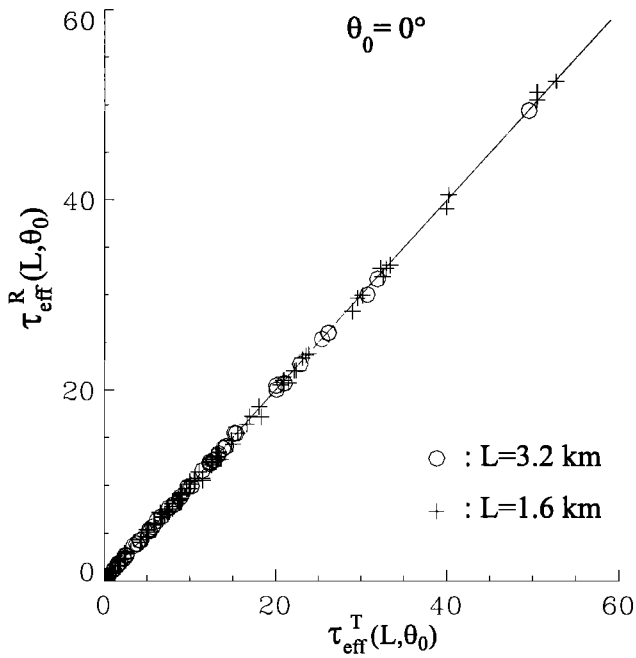

Figure 2. Comparison between τ_{eff}^{R} and τ_{eff}^{T} obtained from the reflectance and transmittance of inhomogeneous cloud segments. Horizontal averaging scale: L = 3.2 km and L = 1.6 km; solar incidence angle $\theta_0 = 0°$.

the horizontal scale of averaging on the effective optical depth, by considering inhomogeneous cloud segments with a horizontal extent L. Then, we will refer to the effective optical depth of such cloud segments as "local effective optical depth" $\tau_{\text{eff}}(L)$.

3.1.2. Dependency of $\tau_{\text{eff}}(L)$ on the horizontal averaging scale. In Figure 2, we plotted $\tau_{\text{eff}}^{R}(L)$ against $\tau_{\text{eff}}^{T}(L)$ for the vertical incidence and for two scales of averaging (3.2 km and 1.6 km). Value $\tau_{\text{eff}}^{R}(L)$ differs little from the corresponding $\tau_{\text{eff}}^{T}(L)$ for both the scales of averaging. This suggests that when vertically illuminated, an inhomogeneous cloud or cloud segment of these horizontal scales can be treated as a PPH cloud if the effective optical depth is used instead of the cloud-mean optical depth. Figure 3, which is the same as Figure 2 but for a solar zenithal angle 30°, exhibits the same general feature of variations except that the dispersion around the bisector is larger in Figure 3 than in Figure 2. The larger dispersion is partly due to an increase in the net horizontal photon transport between the cloud segment and its neighboring cloud pixels with the increasing solar incidence angle.

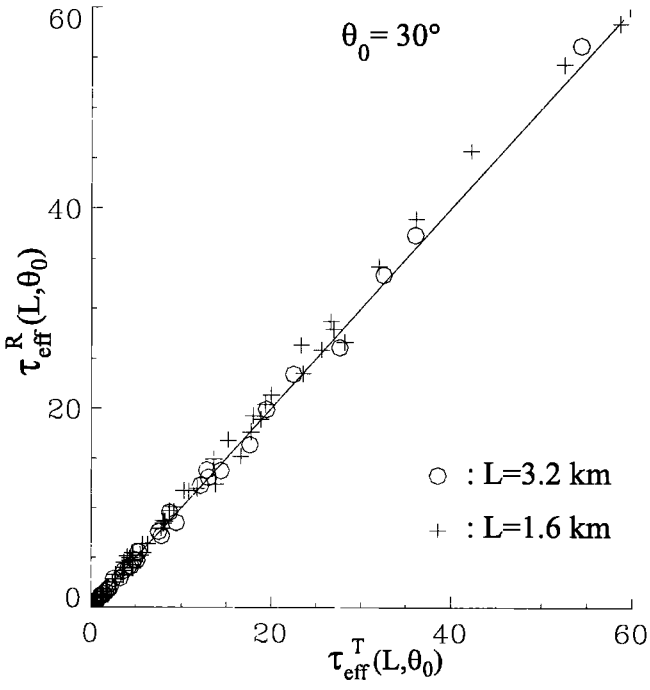

Figure 3. Same as Figure 2 but for $\theta_0 = 30°$.

We defined the relative dispersion as

$$D_{\text{disp}} = \sqrt{\overline{\sin^2 \alpha}} = \left\{ \frac{1}{2N} \sum_{i=1}^{N} \frac{\left[\tau_{\text{eff}}^{R}(i) - \tau_{\text{eff}}^{T}(i)\right]^2}{\left[\tau_{\text{eff}}^{R}(i) + \tau_{\text{eff}}^{T}(i)\right]^2} \right\}^{1/2}, \quad (7)$$

where N is the total number of data. The relative dispersion represents the root-mean-square of $\sin\alpha$, where α is the angle between the vector $(\tau_{\text{eff}}^{R}, \tau_{\text{eff}}^{T})$ and the bisector; we use $(\tau_{\text{eff}}^{R}, \tau_{\text{eff}}^{T})$ instead of $[\tau_{\text{eff}}^{R}(L), \tau_{\text{eff}}^{T}(L)]$ when there is no risk of confusion. Since we were interested in the difference between τ_{eff}^{T} and τ_{eff}^{R}, we preferred to estimate this relative dispersion instead of using the usual linear regression analysis. Another reason for this choice is that the relative dispersion can be easily related to the net horizontal photon transport as shown in section 3.1.4. Table 1 represents the relative dispersions for three incidence angles and five horizontal scales of averaging. We also computed the second estimates of the relative dispersion by using only the data with $\tau_{\text{eff}} \geq 1.5$, because the relative error tends to

Table 1. Relative Dispersion Between τ_{eff}^{T} and τ_{eff}^{R} Around the Bisector as a Function of the Scale of Averaging

	D_{disp} Between τ_{eff}^{T} and τ_{eff}^{R}		
L, km	$\theta_0 = 0°$	$\theta_0 = 30°$	$\theta_0 = 60°$
12.8	7.7×10^{-5}	6.7×10^{-5}	2.2×10^{-5}
	(9.7×10^{-6})	(1.1×10^{-5})	(1.2×10^{-5})
6.4	1.3×10^{-2}	1.8×10^{-2}	5.2×10^{-2}
	(8.1×10^{-3})	(1.9×10^{-2})	(5.4×10^{-2})
3.2	1.8×10^{-2}	5.7×10^{-2}	7.7×10^{-2}
	(9.6×10^{-2})	(3.4×10^{-2})	(8.4×10^{-2})
1.6	4.7×10^{-2}	9.9×10^{-2}	14.0×10^{-2}
	(2.7×10^{-2})	(4.5×10^{-2})	(13.9×10^{-2})
0.8	8.6×10^{-2}	14.2×10^{-2}	18.6×10^{-2}
	(5.1×10^{-2})	(8.2×10^{-2})	(18.4×10^{-2})

Numbers in parentheses are the relative dispersions estimated for $\tau_{\text{eff}} \geq 1.5$.

be larger for small $\tau_{\text{eff}}(L)$ than for moderate to large $\tau_{\text{eff}}(L)$. These estimates are given in parentheses in Table 1.

For the 12.8 km averaging, τ_{eff}^T and τ_{eff}^R of an inhomogeneous cloud should be identical for a given solar incidence angle, because of the periodic lateral boundary conditions. For all the three incidence angles the relative dispersions are close enough to zero. Hence we can conclude that $\tau_{\text{eff}}^T(L)$ and $\tau_{\text{eff}}^R(L)$ of an inhomogeneous cloud are identical at this scale of averaging. For the other scales of averaging the relative dispersion varies significantly with the solar incidence angle; it ranges from about 10^{-2} for $L = 6.4$ km and $\theta_0 = 0°$ to more than 10^{-1} for $L = 1.6$ km and $\theta_0 = 60°$. When the relative dispersion is computed only with the data ($\tau_{\text{eff}} \geq 1.5$), it decreases by about 50% (from 4.7×10^{-2} and 9.9×10^{-2} to 2.7×10^{-2} and 4.5×10^{-2}) for 0° and 30° but remains practically unchanged for 60° (from 14.0×10^{-2} to 13.9×10^{-2}). Accordingly, when the plane-parallel cloud assumption is applied to a given horizontal scale of averaging, its accuracy is strongly dependent on the solar incidence angle.

The relative dispersion D_{disp} may be used as a criterion to define a minimal horizontal averaging scale beyond which the EHCA can be used without any serious error in the radiation budget of an inhomogeneous cloud segment. We hereinafter abbreviate this "minimal scale of averaging" as MSAv. From a practical point of view the determination of the MSAv depends on the errors of the radiant flux we can consider as "acceptable." If we define the MSAv with the criterion $D_{\text{disp}} \leq 5 \times 10^{-2}$, it would be about 1.6 km for 0°, 3.2 km for 30°, and 6.4 km for 60° respectively. The value of $D_{\text{disp}} = 5 \times 10^{-2}$ in the effective optical depth corresponds to a relative error of 5% in the radiative fluxes in the range where the radiative fluxes (reflectance and transmittance) vary quasi-proportionally with the optical depth. For a large optical depth for which the radiative fluxes vary little with the optical depth, $D_{\text{disp}} = 5 \times 10^{-2}$ corresponds to a relative error much less than 5% for the reflectance, while it corresponds to a relative error more than 5% for the transmittance. These MSAvs agree with the horizontal scales of averaging, estimated for the applicability of the plane-parallel cloud assumption by *Barker* [1996].

3.1.3. Dependency of $\tau_{\text{eff}}(L, \theta_0)$ on the solar incidence angle. According to the above results, $\tau_{\text{eff}}^R(L, \theta_0)$ and $\tau_{\text{eff}}^T(L, \theta_0)$ of an inhomogeneous cloud estimated for a given θ_0 are almost identical when they are estimated for a sufficiently large scale of averaging. However, this does not guarantee that $\tau_{\text{eff}}(L, \theta_0)$ is independent of θ_0 , when $\tau_{\text{eff}}(L, \theta_0)$ of the same cloud segment is estimated for different solar incidence angles. Table 2 lists the relative dispersions between $\tau_{\text{eff}}(L, \theta_0)$ and $\tau_{\text{eff}}(L, 0°)$ determined either from the reflectance or the transmittance. As expected, D_{disp} increases with the decreasing scale of averaging and the increasing solar incidence angle. The dispersion is slightly smaller for τ_{eff}^R than for τ_{eff}^T; in other words, photons going through the entire cloud depth are more affected by the cloud inhomogeneity than those reflected from the upper part of clouds; in other words, the net horizontal photon transport does not affect the reflectance and transmittance in the same way. This may have an interesting implication to the cloud parameter retrieval from the up-welling radiation fields.

However, the relative dispersion is too global to analyze in detail how $\tau_{\text{eff}}(L, \theta_0)$ varies with θ_0. Hence we computed the ratio $r(L, \theta_0) = \tau_{\text{eff}}(L, \theta_0)/\tau_{\text{eff}}(L, 0°)$. Figure 4 shows $r(L, 30°)$ and $r(L, 60°)$ of τ_{eff}^R estimated

Table 2. Relative Dispersion Between τ_{eff} for an Oblique Incidence ($\theta_0 = 30°$ and 60°) and τ_{eff} for the Vertical Incidence

	D_{disp} for the Pair			
	$[\tau_{\text{eff}}^T(\theta_0); \tau_{\text{eff}}^T(\theta_0 = 0°)]$		$[\tau_{\text{eff}}^R(\theta_0); \tau_{\text{eff}}^R(\theta_0 = 0°)]$	
L, km	$\theta_0 = 30°$	$\theta_0 = 60°$	$\theta_0 = 30°$	$\theta_0 = 60°$
12.8	5.0×10^{-3}	1.8×10^{-2}	5.0×10^{-3}	1.8×10^{-2}
	(5.0×10^{-3})	(1.8×10^{-2})	(5.0×10^{-3})	(1.8×10^{-2})
6.4	2.6×10^{-2}	3.9×10^{-2}	8.9×10^{-3}	4.1×10^{-2}
	(2.3×10^{-2})	(3.9×10^{-2})	(4.8×10^{-3})	(3.1×10^{-2})
3.2	2.6×10^{-2}	4.4×10^{-2}	1.3×10^{-2}	4.3×10^{-2}
	(1.7×10^{-2})	(4.1×10^{-2})	(1.1×10^{-2})	(3.2×10^{-2})
1.6	2.8×10^{-2}	11.9×10^{-2}	1.8×10^{-2}	5.6×10^{-2}
	(2.7×10^{-2})	(6.5×10^{-2})	(1.7×10^{-2})	(5.3×10^{-2})
0.8	10.3×10^{-2}	18.1×10^{-2}	2.3×10^{-2}	8.3×10^{-2}
	(5.0×10^{-2})	(8.7×10^{-2})	(2.0×10^{-2})	(6.8×10^{-2})

Numbers in parentheses are the relative dispersions estimated for $\tau_{\text{eff}} \geq 1.5$. Effective optical depths are determined either from the reflectance (τ_{eff}^R) or from the transmittance (τ_{eff}^T).

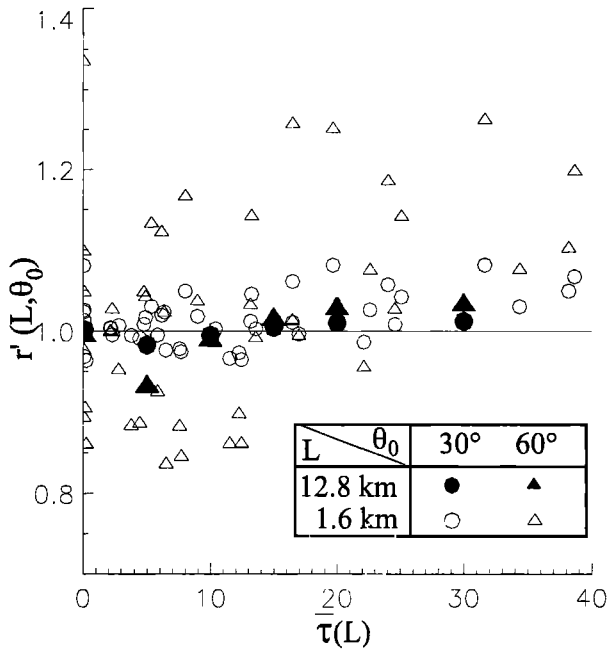

Figure 4. Effect of θ_0 on $r(L, \theta_0) = \tau_{\text{eff}}(L, \theta_0)/\tau_{\text{eff}}(L, 0°)$; $\theta_0 = 30°$ and $\theta_0 = 60°$. Horizontal scale of averaging : $L = 12.8$ km and $L = 1.6$ km.

for two scales of averaging, 12.8 km and 1.6 km, as a function of $\bar{\tau}(L)$. For the 12.8 km averaging, the ratios remain close to 1 for both incidence angles. However, a close examination reveals a slight systematic bias for both incidence angles: for example, $r(12.8\text{ km}, 60°)$ decreases from 1 to about 0.93 as $\bar{\tau}$ increases from 0 to 5, then increases to about 1.03 as $\bar{\tau}$ goes from 5 to 40. For the 1.6 km averaging, $r(1.6\text{ km}, 30°)$ exhibits a similar variation with $\bar{\tau}$, and it goes up to about 1.08 for $20 \leq \bar{\tau}$. Value $r(1.6\text{ km}, 60°)$ is much more scattered; it varies between 0.8 and 1.2 for $\bar{\tau} \leq 10$, while it becomes mostly larger than 1 for $10 \leq \bar{\tau}$. This finding implies that when an inhomogeneous cloud segment with $\bar{\tau} < 10$ is obliquely illuminated, it acts as a cloud segment optically thinner than when it is vertically illuminated, while for $\bar{\tau} \gg 10$, it acts as a cloud segment optically slightly thicker. Consequently, we cannot define, strictly speaking, a unique equivalent homogeneous cloud for a given inhomogeneous cloud, because its effective optical depth would change with the solar incidence angle. However, if the averaging is taken over a sufficiently large area, the solar-incidence-angle dependency of $\tau_{\text{eff}}(L, \theta_0)$ remains small and less than about 3% for most of the mean optical depth except around $\bar{\tau} \approx 5$.

We looked for the explanation of these systematic biases. When a photon with an oblique incidence angle is transmitted through an inhomogeneous cloud layer, this photon follows a slant path through consecutive cloud pixels having different optical depths. The local slant optical depth encountered by this photon can be computed from purely geometrical arguments and converted into an equivalent vertical optical depth as shown in Appendix B. We determined the probability density function (PDF) of this local equivalent vertical optical depth for $\theta_0 = 0°$, 30°, and 60°.

For the homogeneous clouds the PDF is given by a δ function, while for the bounded cascade inhomogeneous clouds, it is close to a lognormal PDF (Figure B1). As θ_0 increases, the PDF of the equivalent vertical optical depth exhibits a significant shift toward a larger optical depth and, at the same time, becomes narrower and skewer to the benefit of large optical depths (Table B1). These features represent the averaging effect of the slant path through an inhomogeneous cloud; these variations of the PDF with the incidence angle occur without any change of the cloud-mean optical depth. They imply that an obliquely penetrating photon encounters more frequently "moderate to large" local optical depth than a vertically penetrating photon. This may explain why $\tau^R_{\text{eff}}(L)$ of an inhomogeneous cloud with a "moderate to large" mean optical depth becomes larger for the oblique incidence than for the vertical incidence. Since the contribution of multiple scattering to the reflectance increases with the cloud-mean optical depth, the above effect would become more effective as the cloud-mean optical depth increases. However, this process cannot be used to explain the opposite effect; that is, the decrease of $r(L, 60°)$ observed for the mean optical depth $\bar{\tau} < 10$. To explain this decrease, we have to consider how the reflectance of the PPH and inhomogeneous clouds varies with $\bar{\tau}$ and θ_0, but also how the difference $R_{\text{hom}}(\bar{\tau}, \theta_0) - R_{\text{inhom}}(\bar{\tau}, \theta_0)$ varies with these parameters. We will resume this discussion after the effect of the net horizontal photon transport is analyzed (equation (12)).

3.1.4. Effect of the net horizontal photon transport on the effective optical depth. A vector $(R_{\text{hom}}, T_{\text{hom}})$ represents a PPH non-absorbing cloud on the (R, T) plane (Figure 5). For the condition of nil net horizontal photon transport, the point $(R_{\text{hom}}, T_{\text{hom}})$ moves on $R + T = 1$ line, as the cloud optical depth varies. In this case, R and T are dependent, and the optical depth can be expressed as a function of either the reflectance $\tau^R = \tau(R_{\text{hom}}; \theta_0)$ or the transmittance $\tau^T = \tau(T_{\text{hom}}; \theta_0)$. The reflectance R_{inhom} and transmittance T_{inhom} of an inhomogeneous cloud with a given $\bar{\tau}$ differ from those of a homogeneous cloud with the same $\bar{\tau}$. The displacement from $(R_{\text{hom}}, T_{\text{hom}})$ to $(R_{\text{inhom}}, T_{\text{inhom}})$ represents the effect of the cloud inhomogeneity. If $R_{\text{inhom}} + T_{\text{inhom}} = 1$, both $\tau^R_{\text{eff}} = \tau(R_{\text{inhom}}; L, \theta_0)$ and $\tau^T_{\text{eff}} = \tau(T_{\text{inhom}}; L, \theta_0)$ still agree with each other.

Let us consider the area-averaged reflectance and transmittance of an inhomogeneous cloud segment such as $R'_{\text{inhom}} + T'_{\text{inhom}} = 1 + \varepsilon$, where the quantity ε indicates an excess or deficit in the radiation budget of the segment due to the net horizontal photon transport into the cloud segment. The displacement from $(R_{\text{hom}}, T_{\text{hom}})$ to $(R'_{\text{inhom}}, T'_{\text{inhom}})$ can be decomposed

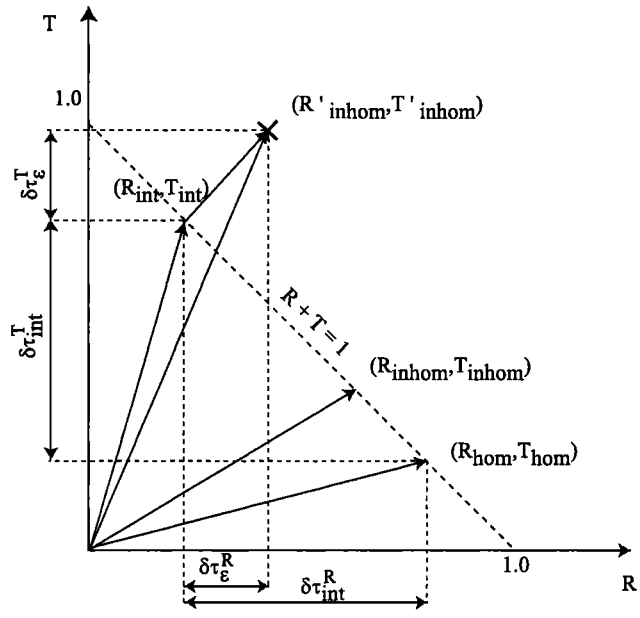

Figure 5. Schematic diagram showing the positions of a homogeneous cloud $(R'_{\rm hom}, T'_{\rm hom})$ and two inhomogeneous clouds with the same mean optical depth: the one having $(R_{\rm inhom}, T_{\rm inhom})$ and the other $(R'_{\rm inhom}, T'_{\rm inhom})$ on the (R,T) plane. The first one has no net horizontal photon transport between the cloud segment and adjacent cloud pixels $R_{\rm inhom} + T_{\rm inhom} = 1$ and the second a finite net horizontal photon transport $R'_{\rm inhom} + T'_{\rm inhom} = 1 + \varepsilon$, where the quantity ε indicates an excess or deficit in the radiative fluxes.

into two displacement vectors, where $(R_{\rm hom}, T_{\rm hom})$ are the reflectance and transmittance of a homogeneous cloud with the same $\bar{\tau}$ as the inhomogeneous cloud. The first displacement is from $(R_{\rm hom}, T_{\rm hom})$ to a point $(R_{\rm int}, T_{\rm int})$ and the second from $(R_{\rm int}, T_{\rm int})$ to $(R'_{\rm inhom}, T'_{\rm inhom})$. The intersection point $(R_{\rm int}, T_{\rm int})$ is determined by drawing the normal from $(R'_{\rm inhom}, T'_{\rm inhom})$ on $R + T = 1$ line (see Figure 5):

$$\begin{cases} R_{\rm int} = \frac{1}{2}[1 + (R'_{\rm inhom} - T'_{\rm inhom})] \\ T_{\rm int} = \frac{1}{2}[1 - (R'_{\rm inhom} - T'_{\rm inhom})]. \end{cases} \tag{8}$$

This decomposition enables us to express the relative dispersion as a simple function of ε. For $\tau^R_{\rm eff}(L)$ we have

$$\delta\tau^R_{\rm eff} = \delta\tau^R_{\rm int} + \delta\tau^R_\varepsilon \tag{9}$$

with

$$\begin{aligned} \delta\tau^R_{\rm eff} &= \tau(R'_{\rm inhom}; L) - \tau(R_{\rm hom}) \\ \delta\tau^R_{\rm int} &= \tau(R_{\rm int}; L) - \tau(R_{\rm hom}) \\ \delta\tau^R_\varepsilon &= \tau(R'_{\rm inhom}; L) - \tau(R_{\rm int}; L). \end{aligned} \tag{10}$$

The first term $\delta\tau^R_{\rm int}$ on the right-hand side represents the variation of the optical depth due to the displacement along $R + T = 1$ line:

$$\delta\tau^R_{\rm int} = \frac{1}{2}\frac{d\tau}{dR}[(R'_{\rm inhom} - T'_{\rm inhom}) - (R_{\rm hom} - T_{\rm hom})]. \tag{11}$$

For $\varepsilon = 0$, equation (9) can be rewritten as

$$\delta\tau^R_{\rm eff} = \delta\tau^R_{\rm int} = -\frac{d\tau}{dR}(R_{\rm hom} - R'_{\rm inhom}). \tag{12}$$

We can use equation (12) to analyze the feature, $r(12.8\ {\rm km}, 60°) < 1$ for $\bar{\tau} < 10$, observed in Figure 4. The difference $(R_{\rm hom} - R'_{\rm inhom})_{\theta=\theta_0}$ is always positive and goes through a maximum at a certain optical depth $\bar{\tau}_{max}(\theta_0)$ as $\bar{\tau}$ increases. When the incidence angle θ_0 increases, $\bar{\tau}_{max}(\theta_0)$ shifts toward a smaller $\bar{\tau}$; this means that for $\bar{\tau} \ll \bar{\tau}_{max}(\theta_0)$, $(R_{\rm hom} - R'_{\rm inhom})_{\theta=60°}$ is larger than $(R_{\rm hom} - R'_{\rm inhom})_{\theta=0°}$. As for $(d\tau/dR)_{\theta=\theta_0}$, $(d\tau/dR)_{\theta=60°}$ is larger than $(d\tau/dR)_{\theta=0°}$ as far as $\bar{\tau}$ is larger than or not much smaller than $\bar{\tau}_{max}(\theta_0)$. Accordingly, we may have $|\delta\tau^R_{\rm eff}(\theta = \theta_0)| > |\delta\tau^R_{\rm eff}(\theta = 0)|$ with $\delta\tau_{\rm eff^R}(\theta = \theta_0) < 0$, if the increase in $(R_{\rm hom} - R'_{\rm inhom})_{\theta=\theta_0}$ overcompensates the decrease in $(d\tau/dR)_{\theta=\theta_0}$ or the decrease in $(R_{\rm hom} - R'_{\rm inhom})_{\theta=\theta_0}$ is compensated by the increase in $(d\tau/dR)_{\theta=\theta_0}$, and this is what happens as shown in Figure 4. Consequently, it is the way in which $(d\tau/dR)_{\theta=\theta_0}$ and $(R_{\rm hom} - R'_{\rm inhom})_{\theta=\theta_0}$ vary with the solar zenith angle, and not the apparent increase in the slant path optical depth, that produces $r(12.8\ {\rm km}, 60°) < 1$ for $\bar{\tau} < 10$ observed on Figure 4. Consequently, the radiative processes that produce $r(12.8\ {\rm km}, 60°) < 1$ feature should be quite different from those contributing to the $1 < r(12.8\ {\rm km}, 60°)$ feature.

As for the second term of equation (9), it represents the variation of the optical depth due to the excess or deficit in the radiation budget of the cloud segment. To estimate this term, we have to choose either reflectance or transmittance:

$$\begin{cases} \delta\tau^R_\varepsilon = (\frac{d\tau}{dR})\frac{\varepsilon}{2} \text{ for } \tau^R_{\rm eff}(L,) \\ \delta\tau^T_\varepsilon = (\frac{d\tau}{dT})\frac{\varepsilon}{2} = -\delta\tau^R_\varepsilon \text{ for } \tau^T_{\rm eff}(L). \end{cases} \tag{13}$$

The vector $(\delta\tau^R_\varepsilon, \delta\tau^T_\varepsilon)$ represents the displacement from the on-bisector point $[\tau(R_{\rm int}, \theta_0), \tau(T_{\rm int}, \theta_0)]$ to the off-bisector point $[\tau(R'_{\rm inhom}, \theta_0), \tau(T'_{\rm inhom}, \theta_0)]$. Consequently, there is no identity between $\tau^R_{\rm eff}(L)$ and $\tau^T_{\rm eff}(L)$ as far as the net horizontal photon transport between the cloud segment and the adjacent cloud pixels is not nil. The relative dispersion defined above can be expressed as:

$$D_{\rm disp} \cong \left\{ \frac{1}{2N} \sum_{i=1}^{N} \frac{[d\,(i)]^2}{[\tau_{\rm eff}\,(i)]^2} \right\}^{1/2} \tag{14}$$

with

$$|d\,(i)| = [(\delta\tau^R_\varepsilon)^2 + (\delta\tau^T_\varepsilon)^2]^{\frac{1}{2}}_i = 2^{\frac{1}{2}} \left| \left(\frac{d\tau}{dR}\right) \frac{\varepsilon}{2} \right|_i, \tag{15}$$

where the index i indicates the ith data point and $\tau_{\rm eff}$ is the effective optical depth. This equation shows that the dispersion depends directly on the ε term.

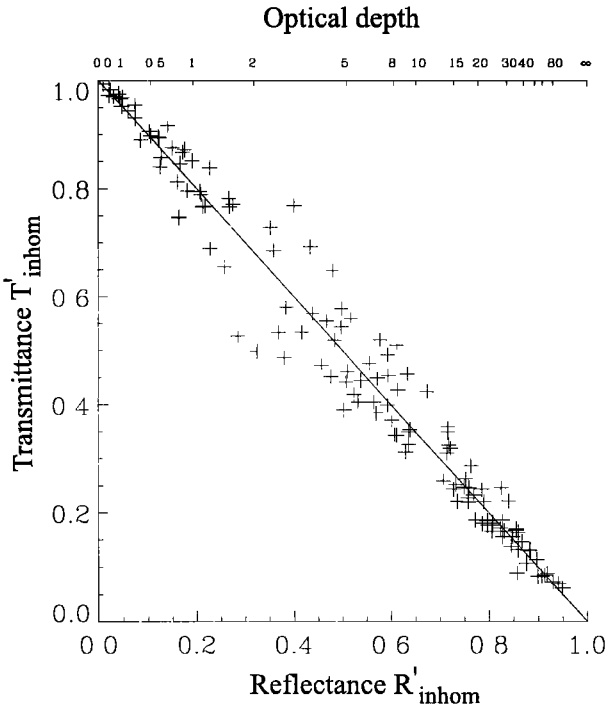

Figure 6. Reflectance R'_{inhom} and transmittance T'_{inhom} of the inhomogeneous cloud segments estimated for the 1.6 km averaging and for the 60° incidence.

Figure 6 shows all pairs $(R'_{\text{inhom}}, T'_{\text{inhom}})$ obtained for inhomogeneous cloud segments with $L = 1.6$ km and $\theta_0 = 60°$. The dispersion around $R + T = 1$, in other words ε term is larger for moderate reflectance or transmittance ($1 < \bar{\tau} < 10$). As T'_{inhom} approaches zero (large $\bar{\tau}$), the penetration depth of photons becomes small. Accordingly, the probability for these photons to participate in the horizontal transport decreases with the penetration depth [*Marshak et al.*, 1998]. This implies that the ε term would become small as $\bar{\tau}$ increases beyond a certain optical depth [*Titov*, 1998]. The dispersion is much smaller for $\theta_0 = 0°$ and 30° (not shown) as expected. The increase in the dispersion with θ_0 may be the result of two factors. The first one is the "resonance" effect on the amplitude of fluctuations (B. Guillemet et al., Effect of cloud inhomogeneity on effective radiative properties, submitted to *Journal of Geophysical Research*, 1999 (hereinafter referred to as G99)). The second one is a phase shift between reflectance and transmittance due to oblique incidence. This phase shift corresponds, in a crude way, to a "geometrical shift" of the directly transmitted ray with respect to its point of entrance, mainly for large values of θ_0.

We evaluated this "geometrical shift" between the reflectance and the transmittance for $\theta_0 = 60°$. This was done by shifting the transmittance with respect to the reflectance and computing the root-mean-square deviation (RMSD) of ε (Figure 7a). We can see a minimum of RMSD for a shift of about 0.35 km; this value is to be compared with the "pure geometrical shift" cloud depth $\times \tan 60° = 0.52$ km . Figure 7 b shows the variation of RMSD we recomputed after shifting the transmittance by 0.35 km. The dispersion in Figure 7 b is much smaller than that in Figure 6. However, there is still a significant residual dispersion, because the value of 0.35 km represents an average shift estimated from all available simulations with different mean optical depths.

3.1.5. Error in the estimation of the transmittance. The above results show that the PPH cloud assumption is only an approximation when applied to an inhomogeneous cloud segment except when the average is taken over the entire cloud domain. Even in this case, we need to neglect the slight dependency of the local effective optical depth on the incidence angle.

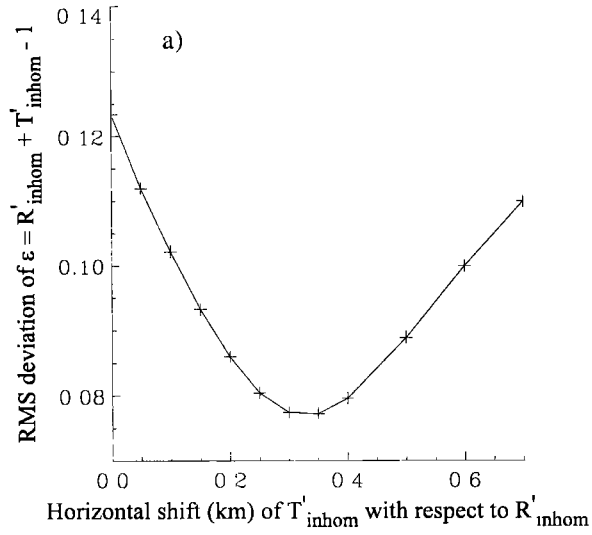

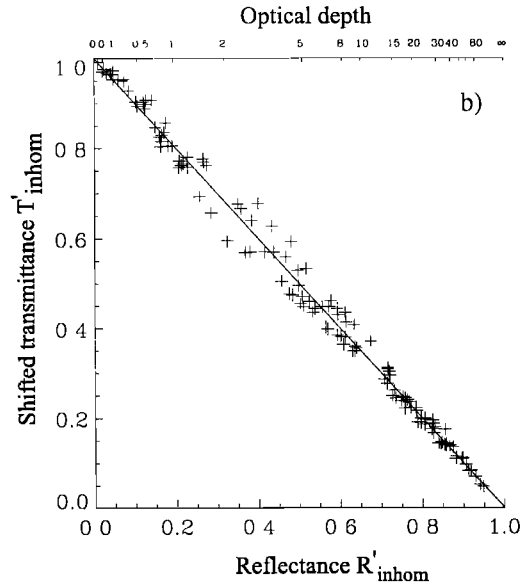

Figure 7. (a) Variation of the RMSD of $\varepsilon = R'_{\text{inhom}} + T'_{\text{inhom}} - 1$ as a function of the horizontal shift of the transmittance T'_{inhom} with respect to the reflectance R'_{inhom}. (b) Same as Figure 6 but after the transmittance T'_{inhom} is shifted horizontally by 0.35 km with respect to the reflectance R'_{inhom} before averaging over 1.6 km.

Let us assume that τ_{eff}^{R} is retrieved from satellite data; we showed that in some conditions the bidirectional reflectance function of inhomogeneous clouds does not differ very much from that of the equivalent plane-parallel homogeneous cloud [*Szczap et al.*, 2000]; consequently, we can extend easily the present result to the radiance measurement. It is important to know what error results on transmittance T . The relative error in T estimated with τ_{eff}^{R} is given by

$$\text{Error}\left[T\left(L\right)\right] \cong \frac{T\left\{\tau\left[R'_{\text{inhom}}\left(L\right)\right]\right\} - T'_{\text{inhom}}\left(L\right)}{T'_{\text{inhom}}\left(L\right)}, \tag{16}$$

where $R'_{\text{inhom}}(L,\theta_0)$ and $T'_{\text{inhom}}(L,\theta_0)$ are the MC reflectance and transmittance of an inhomogeneous cloud segment. Since $T\{\tau[R'_{\text{inhom}}(L,\theta_0),\theta_0]\} = T'_{\text{inhom}}(L,\theta_0) - \varepsilon$ by definition, the relative error can be expressed as

$$\text{Error}[T(L,\theta_0)] = \frac{-\varepsilon}{T'_{\text{inhom}}(L,\theta_0)}. \tag{17}$$

This error is plotted versus τ_{eff}^{R} for $\theta_0 = 0°$, 30°, 60° (Figures 8a, 8b, 8c). The relative error is bounded as τ_{eff} increases, because there is a compensation between the decreases of ε and $\tau_{\text{eff}}^{R}(\theta_0)$. As expected, it is strongly dependent on θ_0, from less than 5% for the vertical incidence to 7% and 20% for 30° and 60° when averaged over $L = 1.6$ km. Doubling L to 3.2 km brings in only a slight improvement. The variation of the relative error with the averaging scale bears out the MSAv values proposed in subsection 3.1.2. Indeed, the transmittance can be obtained with a relative error less than 5% for $0° \leq \theta_0 \leq 30°$ provided that $L \geq 3.2$ km; this corresponds to an aspect ratio of the cloud segment (aspect ratio = $\frac{\text{horizontal length}}{\text{vertical thickness}}$) about 10. $L \geq 6$ km

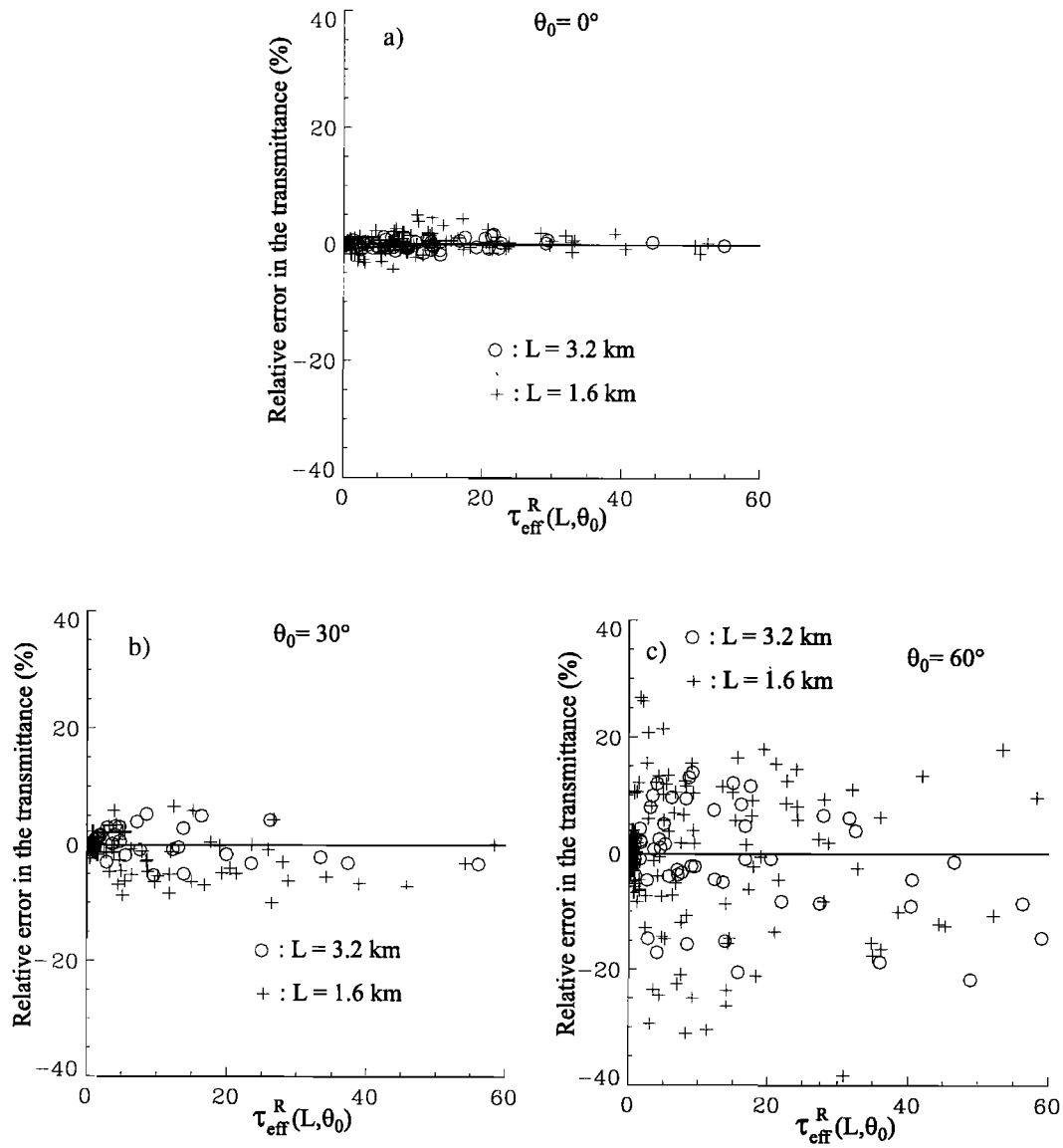

Figure 8. Effect of the incidence angle on the relative error in the transmittance when $\tau_{\text{eff}}^{R}(L)$ is used for $\tau_{\text{eff}}^{T}(L)$. Incidence angles: (a) $\theta_0 = 0°$; (b) $\theta_0 = 30°$; (c) $\theta_0 = 60°$. Horizontal scale of averaging: circles , $L = 3.2$ km; pluses : $L = 1.6$ km.

would be required for the same error for $\theta_0 = 60°$. This means that τ_{eff}^R may introduce a significant error in the estimation of transmittance, even if the transmittance is estimated at an aspect ratio of as large as 20.

3.2. Relation Between τ_{eff} and Local Cloud Properties

In analyzing the dependency of τ_{eff} on the local mean optical depth and scale of averaging, we have to use, in principle, only τ_{eff} estimated for cloud segments with a horizontal extent larger than the MSAv, i.e., a small contribution of ε term. However, this would limit considerably the scope of the present analysis, because only few τ_{eff} satisfy such a condition for the 30° and 60° incidences. Hence we considered all τ_{eff} estimated for the scales of averaging larger than or equal to 1.6 km, even if this results in a larger dispersion.

Since τ_{eff} is a quasi-linear function of $\bar{\tau}$, we computed the ratio between these two optical depths: $r'(L,\theta_0) = \tau_{\text{eff}}(L,\theta_0)/\bar{\tau}(L)$, and plotted it as a function of $\bar{\tau}$. Figure 9 represents $r'(L,\theta_0)$ computed for two averaging scales, 12.8 km and 1.6 km,respectively and for two incidence angles, 0° and 60°, respectively. It clearly shows the dependency of $r'(L,\theta_0)$ on the local mean optical depth, but also on the horizontal scale of averaging. The dependency on the scale of averaging occurs because the "degree of inhomogeneity" depends on the averaging scale, whatever the exact meaning of the "degree of inhomogeneity" is.

For a large mean optical depth the ratio approaches an asymptotic value β, so we have approximately

$$\tau_{\text{eff}}(L,\theta_0) = \beta\,\bar{\tau}(L). \tag{18}$$

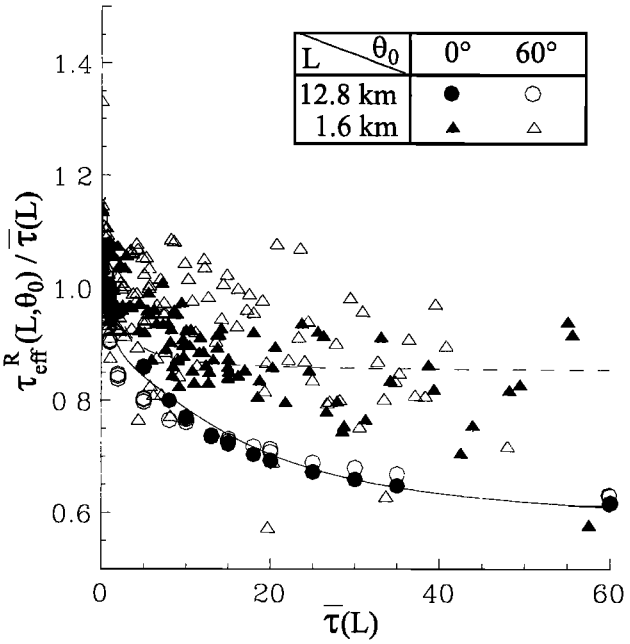

Figure 9. Variation of $r'(L,\theta_0) = \tau_{\text{eff}}(L,\theta_0)/\bar{\tau}(L)$ as a function of the local mean optical depth $\bar{\tau}(L)$; solar incidence angle: $\theta_0 = 0°$ and $\theta_0 = 60°$. Horizontal averaging scale: $L = 12.8$ km and $L = 1.6$ km.

This is evident for the 12.8 km averaging, while for 1.6 km, it is much less evident due to a large dispersion of the estimated ratios. *Cahalan et al.* [1994a] proposed a similar expression with a constant coefficient of $\beta = 0.7$ for an inhomogeneous cloud with a mean optical depth of about 13. For the 12.8 km averaging, $r'(L,\theta_0)$ decreases from 1.0 at $\bar{\tau} = 0$ to about 0.63 at $\bar{\tau} \geq 60$. We find $\beta \cong 0.75$ for $\bar{\tau} = 13$, which corresponds approximately to $\beta = 0.7$ given by Cahalan et al. Figure 9 shows that τ_{eff} under the EHCA differs from τ_{eff} defined under the ETA by more than 20% for small mean optical depth and by more than 10% for large mean optical depth.

In spite of a larger dispersion we can remark that the coefficient β approaches to 1, on average, as the scale of averaging decreases. This occurs because the standard deviation of fluctuations in the optical depth decreases with the decreasing scale of averaging, due to the -1.5 spectral slope of the optical depth fluctuations. When the averaging scale is smaller than the MSAv, the dispersion of $r(L,\theta_0)$ is quite important because of a significant variability of local inhomogeneity from one cloud segment to another. Another reason for this large dispersion is the contribution of the ε term, which is due to the nonzero net horizontal photon transport between the cloud segment and the adjacent cloud pixels.

We defined a local relative cloud-inhomogeneity parameter as $\rho_\tau(L) = \sigma_\tau(L)/\bar{\tau}(L)$, where $\sigma_\tau(L)$ and $\bar{\tau}(L)$ designate, respectively, the local standard deviation of optical depth fluctuations and the local mean optical depth over a cloud segment of L . The reason for this choice is that as the mean optical depth $\bar{\tau}(L)$ varies, the same $\sigma_\tau(L)$ does not have the same effect on the radiant flux components, i.e., the reflectance and transmittance of the cloud segments. The square of this local relative cloud-inhomogeneity parameter is the inverse of the cloud-inhomogeneity parameter proposed independently in the gamma IPA by *Barker* [1996b]. However, its use in this study is significantly different from that of Barker's work. The present results show that the relative cloud inhomogeneity is scale-dependent, and this may have important consequences in analyzing experimental data obtained at different scales of averaging.

An empirical relation between $\tau_{\text{eff}}(L)$ and $\bar{\tau}(L)$ has to satisfy the following conditions:

$$\begin{aligned} \tau_{\text{eff}}(L) &= \bar{\tau}(L) \text{ as } \rho_\tau(L) \to 0, \\ \tau_{\text{eff}}(L) &= \bar{\tau}(L) \text{ as } \bar{\tau}(L) \to 0. \end{aligned} \tag{19}$$

The first condition means that when the relative cloud-inhomogeneity parameter goes down to zero, an inhomogeneous cloud segment behaves as a homogeneous cloud with the same local mean optical depth. The second condition, independent from the first one, implies that the cloud inhomogeneity should have no effect when the mean optical depth becomes very small (Figure 9).

We determined an empirical relation for τ_{eff} by fitting the data points to the following function:

$$\tau_{\text{eff}}^{\text{cal}} = \left\langle A\frac{1+B\bar{\tau}}{1+C\bar{\tau}}[1-\exp(D\rho_\tau)] + \bar{\tau}\{1+E[1-\exp(F\rho_\tau)]\}\right\rangle \cdot \left\langle 1-\exp\left\{-\frac{\bar{\tau}}{A[1-\exp(D\rho_\tau)]}\right\}\right\rangle, \quad (20)$$

where the constants are $A = -4.53 \times 10^{-3}$, $B = 1.57 \times 10^{-1}$, $C = 2.64 \times 10^{-1}$, $D = 12.6$, $E = 5.68 \times 10^{-2}$, and $F = 3.78$, respectively. This equation is of the same type as the one proposed by *Borde and Isaka* [1996]. Equation (20) enables us to calculate $\tau_{\text{eff}}^{\text{cal}}$ of an inhomogeneous cloud segment as a function of $\bar{\tau}(L)$ and $\rho_\tau(L)$. The spatial correlation of the fluctuations, i.e., the spectral slope of fluctuations, is not explicitly included in equation (20). This does not exclude a possibility that the constants A, B, C, D, E, and F may depend on the spectral slope.

Figure 10 compares $\tau_{\text{eff}}^{\text{cal}}$ calculated with equation (20) with τ_{eff}^{R} estimated from Monte Carlo reflectance. Value $\tau_{\text{eff}}^{\text{cal}}$ agrees fairly well with τ_{eff}^{R}, and we obtained a relative dispersion of $D_{\text{disp}} = 3.6 \times 10^{-2}$ for them. The difference between $\tau_{\text{eff}}^{\text{cal}}$ and τ_{eff}^{R} results from three distinct causes: (1) the adjustment of data to the function we chose to fit, (2) the nonzero net horizontal photon transport, and (3) the error in the estimation of τ_{eff}^{R}, in particular large τ_{eff}^{R}. However, as far as the effect of net horizontal photon transport is small ($\tau_{\text{eff}}^{R} \simeq \tau_{\text{eff}}^{T}$), we could fit, in principle, these data to other types of function instead of the above function and improve the degree of approximation by including explicitly the incidence angle dependency of the effective optical depth if necessary.

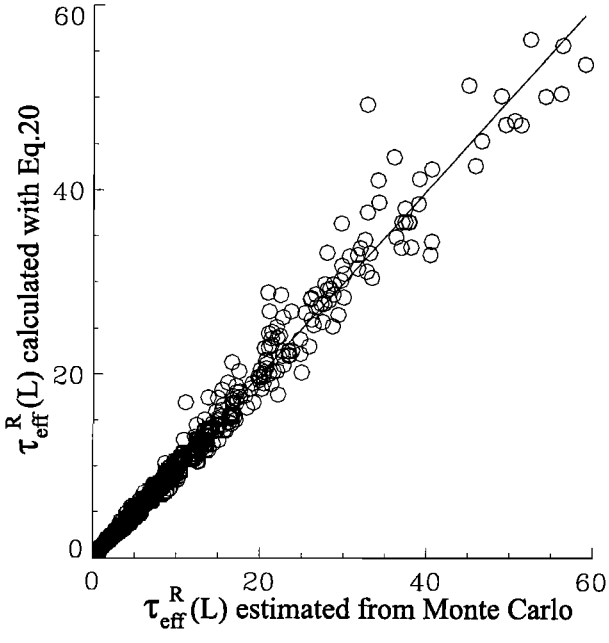

Figure 10. Comparison between τ_{eff}^{R} estimated from the reflectance and $\tau_{\text{eff}}^{\text{cal}}$ calculated from equation (20) for cloud segments with different scales and different incidence angles. The local cloud inhomogeneity $\rho_\tau(L)$ and local mean optical depth $\bar{\tau}(L)$ estimated for each cloud segment are used in equation (20).

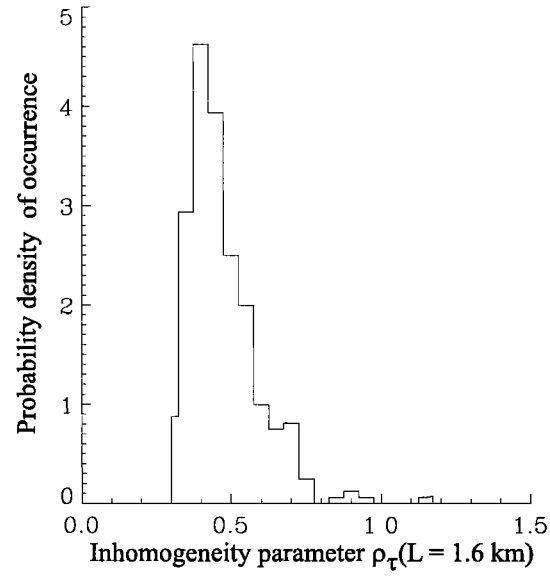

Figure 11. Distribution of the relative frequency of occurrence of the inhomogeneity parameter $\rho_\tau(L)$ (horizontal scale of averaging, $L = 1.6$ km).

The relative cloud-inhomogeneity parameter of a cloud segment varies around its mean value $\overline{\rho_\tau(L)}$ from one cloud segment to another. Figure 11 shows the probability distribution of $\rho_\tau(1.6$ km), which varies from 0.3 to 0.7 with a long tail up to 1.2. Relatively large values obtained for $\rho_\tau(1.6$ km) can be explained by the limited number of cascades we used. Since the standard deviation of $\rho_\tau(L)$ is small compared with $\overline{\rho_\tau(L)}$, we may calculate $\tau_{\text{eff}}^{\text{cal}}$ with $\overline{\rho_\tau(L)}$ in equation (20) instead of $\rho_\tau(L)$. The relative dispersion D_{disp} increases slightly from 3.6×10^{-2} to 4.3×10^{-2}; this indicates that the mean relative cloud-inhomogeneity might be used sometimes instead of the local relative cloud inhomogeneity without much loss of accuracy.

The above results indicate that the effect of cloud inhomogeneity on the radiant flux varies with the scale of averaging, because of the scale dependency of the cloud-inhomogeneity parameter. Hence it is important to take account of the relative cloud-inhomogeneity parameter compatible with the scale of averaging, when we want to parameterize the effective optical depth. This constitutes a significant difference from the effective optical depth defined as a function of the fractal parameters at the cloud domain scale in the works of *Cahalan et al.* [1994a] and *Borde and Isaka* [1996].

Some dispersion remains for the 1.6 km averaging, because there are various factors that cannot be completely taken into account in equation (20). For example, the use of $\bar{\tau}(L)$ and $\rho_\tau(L)$ in equation (20) assumes that the reflectance and transmittance of a cloud segment are completely conditioned by the optical and structural characteristics of the cloud segment itself.

Furthermore, in the above analysis we used all available $\tau_{\text{eff}}^{R}(L)$ estimated for the scales of averaging larger than or equal to 1.6 km and for all incidence angles, which results necessarily in a larger dispersion.

As already shown above, the contribution of the ε term becomes more important for small L than for large L, but also for small $\tau_{\text{eff}}(L)$ than for large $\tau_{\text{eff}}(L)$. This explains why $\tau_{\text{eff}}^{R}(L)$ becomes sometimes larger than $\bar{\tau}(L)$ and more frequently, for the 60° incidence than 0° incidence. The contribution of adjacent cloud pixels cannot be, by its principle, taken account of and corrected in the framework of the approach developed in the present paper. The effect of neighboring cloud pixels on the radiant flux of the cloud segments can be treated partially with the NIPA. We will discuss this problem in detail elsewhere (T. Faure et al., Neural network analysis of the radiative interaction between neighboring cloud pixels of inhomogeneous cloud, submitted to *Journal of Geophysical Research*, 1999a (hereinafter referred to as F99a); T. Faure et al., Application of mapping network to compute radiant flux of inhomogeneous clouds at cloud pixel size, submitted to *Journal of Geophysical Research*, 1999b (hereinafter referred to as F99b)).

3.3. Comparison of the EHCA With the IPA and ETA

In many recent studies the IPA and its variants were applied to study the effect of cloud inhomogeneity on the radiative flux. They appear as a "standard method" to deal with the radiative transfer in inhomogeneous clouds, at least to calculate their radiant flux components [*Cahalan et al.*, 1994b; *Marshak et al.*, 1995b, 1998; *Barker*, 1996b]. Since the EHCA deals with an inhomogeneous-cloud segment as well as with a cloud domain, it covers the spatial scales considered separately by the IPA and NIPA under a unique framework.

When the IPA or NIPA and the ETA or EHCA are applied to calculate the reflectance of inhomogeneous nonabsorbing clouds as "direct problem," there is no significant difference in their practical performance. This implies, as already said, that the nonlinear effect of "radiative transfer-cloud inhomogeneity" interaction is not important for the bounded cascade nonabsorbing clouds when the radiant flux components are averaged over a large enough area. All of them require "a priori" knowledge of the cloud inhomogeneity. However, there is an important difference in the required knowledge of cloud inhomogeneity, i.e., local fluctuations of the optical depth at one cloud pixel with about 10 m wide for the IPA and NIPA and the relative cloud inhomogeneity for the ETA and EHCA. It is interesting to remark that the gamma IPA bypasses the knowledge of local fluctuations of the optical depth by assuming their probability distribution.

The application of the IPA or NIPA to the downward radiance might not be so easy as its application to the upward radiance, because the net horizontal photon transport between adjacent pixels does not affect the downward flux in the same way as the upward flux. The phase shift between the transmittance and the reflectance for the oblique incidence illustrates this problem (G99, F99a). Furthermore, when the IPA or gamma IPA is applied to the transmittance, its performance is only a by-product of its performance in approximating the reflectance.

The EHCA can be considered as a variant of the ETA proposed by *Cahalan et al.* [1994a]. Hence it is important to clarify the difference between them, even though the difference between them would be better clarified when applied to the absorbing inhomogeneous clouds [*Szczap et al.*, this issue]. The ETA was proposed by defining an effective optical depth through the area-averaged IPA reflectance. The IPA reflectance of each cloud pixel is considered as a function of $\ln\tau$ instead of τ, and its Taylor expansion around the point $\overline{\ln\tau}$ is averaged over the entire cloud domain:

$$\overline{R(\ln\tau)} = R\left(\overline{\ln\tau}\right) + \left[\frac{\partial R}{\partial(\ln\tau)}\right]_{\overline{\ln\tau}} \overline{\delta\ln\tau} + \frac{1}{2}\left[\frac{\partial^2 R}{\partial(\ln\tau)^2}\right]_{\overline{\ln\tau}} \overline{(\delta\ln\tau)^2} + \ldots \quad (21)$$

where $R(\ln\tau)$ represents the IPA reflectance and $\delta\ln\tau$ represents the difference $\ln\tau - \overline{\ln\tau}$. For $[\frac{\partial^2 R}{\partial(\ln\tau)^2}]_{\overline{\ln\tau}} = 0$, the arithmetic mean of the reflectance on the left-hand side can be approximated by the reflectance of a homogeneous cloud with an optical depth of $\tilde{\tau}$, where $\tilde{\tau}$ defined as $\ln\tilde{\tau} = \overline{\ln\tau}$ represents a geometrical mean of optical depth over the entire cloud domain. Since we have $\overline{\ln\tau} = \ln(\beta\bar{\tau})$ for the bounded cascade model at the scale of the entire cloud domain, the effective optical depth at the scale of the entire cloud domain can be expressed by a linear function of the mean optical depth: $\tau_{\text{eff}} = \tilde{\tau} = \beta\bar{\tau}$.

It should be remarked, however, that this effective optical depth is exact only for a unique mean optical depth, at which the second-order derivative can be neglected. For other mean optical depths the ETA represents only an approximation to the "true" effective optical depth defined in this present study. Furthermore, the constant β is relevant only to the cascade process used to generate the inhomogeneous clouds and to the scale of entire cloud domain. It can be applied neither to an inhomogeneous cloud generated by other processes nor to an inhomogeneous cloud segment. Compared with the effective optical depth of the ETA, the effective optical depth under the EHCA varies with $\bar{\tau}(L)$, but also with the local cloud inhomogeneity. This dependency on the local cloud inhomogeneity constitutes one of the differences between the EHCA and the ETA based on the IPA. Accordingly, the EHCA seems to provide a rational framework to discuss how cloud inhomogeneity affects the radiant flux and at what horizontal scale the PPH cloud assumption becomes valid without any serious error.

One of the practical utilities of the EHCA is that the effective optical depth or other effective cloud properties are expressed as a function of in situ measurable cloud properties: the effective optical depth is expressed as a function of the local mean optical depth $\bar{\tau}(L)$ and local relative cloud inhomogeneity $\rho_\tau(L)$. Such an empirical relation is needed to interpret the effective cloud parameters that can be retrieved from remotely sensed radiometric data, in terms of in situ measured cloud parameters such as the mean optical depth, cloud inhomogeneity, etc (F99c).

4. Conclusion

In this paper we investigated the effect of the subcloud scale inhomogeneity on the radiative properties of inhomogeneous clouds under the equivalent homogeneous cloud approximation. In doing so, we defined a plane-parallel homogeneous cloud equivalent to a given inhomogeneous cloud and determined its effective cloud parameters by requiring the identity of its radiant flux components between these clouds.

The present study shows that the effective radiative properties of an inhomogeneous cloud depend significantly on the scale of averaging. Accordingly, we should take into account an appropriate degree of cloud inhomogeneity in computing the area-averaged radiant flux as a function of the area-averaged radiative properties. This also implies a need to correct the cloud inhomogeneity effect on the retrieved cloud parameters if we intend to compare satellite-retrieved cloud parameters with in situ measured cloud parameters.

The present study also suggests that the application of the plane-parallel cloud assumption for the cloud parameter retrieval should not be equated with its use for the estimation of a radiation budget of inhomogeneous clouds. Indeed, the effective optical depth estimated from the reflectance does not vary very much with the incidence angle, even if the horizontal scale of averaging is significantly less than the MSAv. However, this does not imply that we could apply the plane-parallel homogeneous cloud assumption for the estimation of the radiation budget at this horizontal scale of averaging. A very large scale of averaging that corresponds to an aspect ratio much larger than 20 is needed to apply the plane-parallel homogeneous cloud assumption to the flux estimation in order to compensate the effect of horizontal shift between the reflectance and transmittance for a large incidence angle.

The EHCA assumes that the reflectance and transmittance of a cloud segment are completely determined by its optical and structural characteristics. When this condition is not satisfied because of the nonzero net photon transport, the present method cannot correct, by its principle, the contribution of adjacent cloud pixels. However, the EHCA enables us to minimize the error in the estimation of individual local radiative flux. In spite of these limitations an empirical relation such as equation (20) provides us with interesting information about the effect of cloud inhomogeneity on the aggregation of satellite data having different pixel sizes.

When inhomogeneous clouds are generated with other processes than the bounded cascade process, it is possible that most of the present results stand qualitatively without major modification, but change quantitatively. Consequently, we need to investigate how the effective optical properties of an inhomogeneous medium as well as the scaling of radiative transfer in such a medium may be influenced by the types of cloud inhomogeneity. This implies that we have to look for a more general approach to generate a stochastically inhomogeneous cloud or cloud field with statistical characteristics of natural clouds.

Appendix A: Monte Carlo Intrinsic Errors

The Monte Carlo method has an intrinsic statistical error, which decreases when increasing the number of photons. *Cahalan et al.* [1994b] proposed to estimate the intrinsic relative error E in the radiative flux as $E \approx [(N_0 - N_r)/(N_0 N_r)]^{1/2}$, N_0 and N_r being, respectively, the total number of incident photons and the number of photons contributing to the specific radiative flux. This expression may also provide the upper bound of the relative error in the radiative flux of inhomogeneous clouds.

Table A1. Relative Intrinsic Error in the Reflectance and Transmittance for a Cloud Pixel 50 m Wide and a Cloud Segment (16 Cloud Pixels) for the 0 Incidence

	Cahalan's Formula		From Simulated Fluxes	
Mean Optical Depth	Cloud Pixel Reflectance (16 Cloud Pixels)	Cloud Pixel Transmittance (16 Cloud Pixels)	Cloud Pixel Reflectance (16 Cloud Pixels)	Cloud Pixel Transmittance (16 Cloud Pixels)
$\bar{\tau} = 5$	4.5×10^{-3}	1.9×10^{-3}	5.6×10^{-3}	3.6×10^{-3}
	(1.1×10^{-3})	(4.6×10^{-4})	(1.7×10^{-3})	(8.7×10^{-4})
$\bar{\tau} = 20$	2.1×10^{-3}	4.2×10^{-3}	3.5×10^{-3}	5.1×10^{-3}
	(5.1×10^{-4})	(1.0×10^{-3})	(1.4×10^{-3})	(1.5×10^{-3})

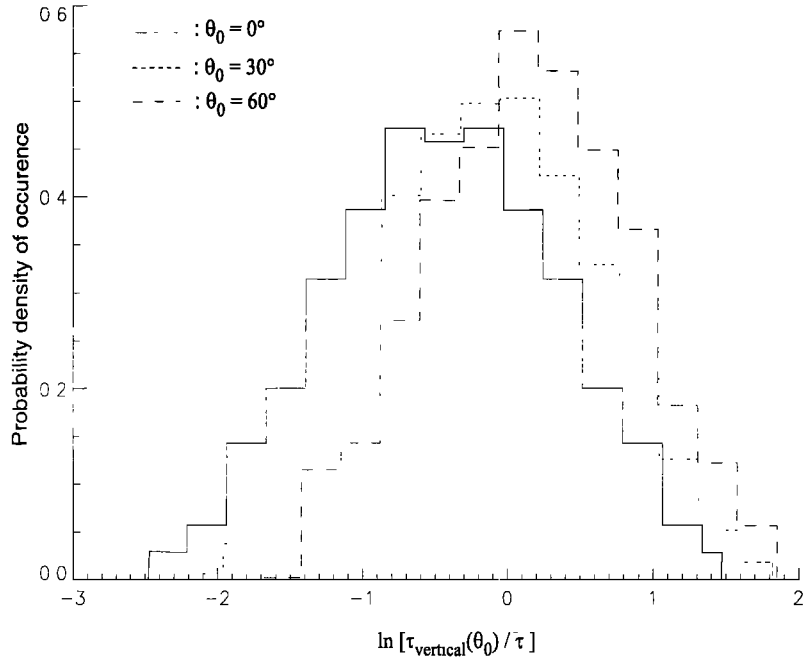

Figure B1. Probability density function of the vertically equivalent optical depth sawn by a θ_0 incidence photon transmitted directly though an inhomogeneous bounded cascade cloud layer ($H = 0.5; 2p = 0.5$). Solar incidence angle: $\theta_0 = 0°$, 30°, and 60°.

We estimated the statistical error of the Monte Carlo method in two ways: (1) using the above expression and (2) computing the statistics from simulations obtained for homogeneous clouds. Table A1 shows the relative error in the reflectance and transmittance, respectively, for a cloud pixel 50 m wide and a cloud segment of 0.8 km (corresponding to 16 cloud pixels) for normal incidence. The average number of photons is 1.2×10^5 per pixel.

The relative error calculated with the above formula is always smaller than those estimated from simulations by about 50%. This discrepancy between the two estimates may be explained by considering that the horizontal photon transport between a cloud segment and its adjacent cloud pixels cannot be neglected at these small scales (1 and 16 cloud pixels), while the above formula assumes implicitly zero net horizontal photon transport between the cloud segment and the neighboring cloud pixels.

Appendix B: The Probability Density Function of the Optical Depth of Inhomogeneous Clouds for the Vertical and Oblique Incidence

The probability density function of local optical depth is one of the important factors governing the interaction between radiative transfer and inhomogeneous cloud. When a photon enters the ith cloud pixel with an incidence angle θ_0, it will schematically follow a slant path through p consecutive cloud pixels. We can compute a local oblique optical depth for this photon with oblique incidence from purely geometrical arguments. The vertically equivalent optical depth corresponding to this slant path is given as $\tau_{\text{vertical}}(\theta_0) = \sum_{k=i}^{i+p-1} \Delta\tau_k$, with $\Delta\tau_k$ for the local equivalent vertical optical depth corresponding to the slant path through the kth cloud pixel. By computing this equivalent vertical optical depth successively for each pixel of the cloud, we obtain the prob-

Table B1. Mean Value, Standard Deviation, and Skewness of $\ln[\tau_{\text{vertical}}(\theta_0)/\bar{\tau}]$ and $\tau_{\text{vertical}}(\theta_0)/\bar{\tau}$ for $\theta_0 = 0°$, 30°, and 60°

	$\ln[\tau_{\text{vertical}}(\theta_0)/\bar{\tau}]$			$\tau_{\text{vertical}}(\theta_0)/\bar{\tau}$		
	Mean	σ	S_k	Mean	σ	S_k
$\theta_0 = 0°$	−0.30	0.78	1.1×10^{-8}	1.00	0.84	1.74
$\theta_0 = 30°$	−0.26	0.73	-0.5×10^{-2}	1.00	0.77	1.37
$\theta_0 = 60°$	−0.23	0.68	-1.7×10^{-2}	1.00	0.70	1.05

ability density function of optical depth of a bounded cascade inhomogeneous cloud for an oblique incidence.

Figure B1 represents the probability density functions for incidence angles of 0°, 30°, and 60°. A logarithmic scale $\ln[\tau_{\text{vertical}}(\theta_0)/\bar{\tau}]$ is used, because the probability density function of $\bar{\tau}$ of a bounded cascade cloud for the vertical incidence is close to the lognormal distribution [*Cahalan et al.*, 1994]. Table B1 represents the mean value, standard deviation and skewness of $\ln[\tau_{\text{vertical}}(\theta_0)/\bar{\tau}]$ and $\tau_{\text{vertical}}(\theta_0)/\bar{\tau}$ for the three incidence angles.

Acknowledgments. This investigation was conducted jointly under Japanese Space Agency (NASDA) grant, GLI/ADEOS II project G-0033, and the French National Institute for Sciences of the Universe (INSU) grant, 96/ATP/494/220.2.

References

Aida, M., Scattering of solar radiation as a function of cloud dimension and orientation, *Quat. Spectrosc. Radiat. Transfer*, *17*, 303-310, 1977.

Barker, H. W., Solar radiative transfer through clouds possessing isotropic variable extinction coefficient, *Q. J. R. Meteoral. Soc.*, *118*, 1145-1162, 1992.

Barker, H. W., Solar radiative transfer for wind-sheared cumulus cloud fields, *J. Atmos. Sci.*, *51*, 1141-1156, 1994.

Barker, H. W., Estimating cloud field albedo using one-dimensional series of optical depth, *J. Atmos. Sci.*, *53*, 2826-2837, 1996a.

Barker, H. W., A parameterization for computing Grid-Averaging solar fluxes for inhomogeneous marine boundary layer cloud., part I, Methodology and homogeneous biases, *J. Atmos. Sci.*, *53*, 2289-2303, 1996b.

Barker, H. W., and J. A. Davies, Cumulus cloud radiative properties and the characteristics of satellite wave-number spectra, *Remote. Sens. Environ.*, *42*, 51-64, 1992.

Barker, H. W., B. A. Wielicki, and L. Parker, A parameterization for computing grid-averaging solar fluxes for inhomogeneous marine boundary layer cloud, part II, Validation using satellite data, *J. Atmos. Sci.*, *53*, 2304-2316, 1996.

Borde, R., and H. Isaka, Radiative transfer in multifractal clouds, *J. Geophys. Res.*, *101*, 29,461-29,478, 1996.

Bréon, F. M., Reflectance of broken cloud fields, Simulation and parameterization, *J. Atmos. Sci.*, *49*, 1221-1232, 1992.

Cahalan, R. F., Overview of fractal clouds, *in Advances in Remote Sensing Retrieval Methods*, pp. 371-388, A. Deepak, Hampton, Va., 1989.

Cahalan, R. F., and J. B. Snider, Marine stratocumulus structure, *Remote Sens. Environ.*, *28*, 95-107, 1989.

Cahalan, R. F., W. Ridgway, W. J. Wiscombe, T. L. Bell, and J. B. Snider, The albedo of fractal stratocumulus clouds, *J. Atmos. Sci.*, *51*, 2434-2455, 1994a.

Cahalan, R. F., W. Ridgway, W. J. Wiscombe, S. Gollmer, and Harshvardhan, Independent pixel and Monte Carlo estimates of stratocumulus albedo, *J. Atmos. Sci.*, *51*, 3776-3790, 1994b.

Chambers, L. H., B. A. Wielicki, and K. F. Evans, Independent pixel and two-dimensional estimates of Landsat-derived cloud field albedo, *J. Atmos. Sci.*, *54*, 1525-1532, 1997.

Davies, R., The effect of finite geometry on the three-dimensional transfer of solar irradiance in clouds, *J. Atmos. Sci.*, *35*, 1712-1725, 1978.

Davies, R., W. L. Ridgway, and K. E. Kim , Spectral absorption of solar radiation in cloudy atmospheres: A 20 cm^{-1} model, *J. Atmos. Sci.*, *41*, 2126-2137, 1984.

Davis, A., S. Lovejoy, and D. Schertzer, Discrete angle radiative transfer in multifractal medium, *SPIE Proc.*, *1558*, 51-64, 1991.

Davis, A., A. Marshak, W. Wiscombe, and R. Cahalan, Multifractal characterizations of nonstationarity and intermittency in geophysical fields, observed, retrieved or simulated, *J. Geophys. Res.*, *99*, 8055-8072, 1994.

Davis, A., A. Marshak, W. J. Wiscombe, and R. Cahalan, Scale invariance of liquid water distributions in marine stratocumulus, Part I, Spectral properties and stationarity issues, *J. Atmos. Sci.*, *53*, 1538-1568, 1996.

Davis, A., A. Marshak, R. Cahalan, and W. J. Wiscombe, The Landsat scale break in stratocumulus as a three-dimensional radiative transfer effect: Implication for cloud remote sensing, *J. Atmos. Sci.*, *54*, 241-260, 1997.

Davis, A., A. Marshak, H. Gerber, and W. J. Wiscombe, Horizontal structure of marine boundary clouds from centimeter to kilometer scales, *J. Geophys. Res.*, *104*, 6123-6144, 1999.

Duroure, C., and B. Guillemet, Analyses des hétérogénéités spatiales des stratocumulus et cumulus, *Atmos. Res.*, *25*, 331-350, 1990.

Garcia, R., and C. Siewert, Benchmark results in radiative transfer, *Transp. Theor. Stat. Phys.*, *14*, 437-484, 1985.

Lovejoy, S., Area-parameter relation for rain arid clouds areas, *Science*, *216*, 185-187, 1982.

Marchuk, G., G. Mikhailov, M. Nazaraliev, R. Darbinjanl, B. Kargin, and B. Elepov, *The Monte Carlo Methods in Atmospheric Optics*, 208 pp., Springer-Verlag, New York, 1980.

Marshak, A., A. Davis, R. Cahalan, and W. Wiscombe, Bounded cascade models as non-stationary multifractals, *Phys. Rev. E*, *49*, 55-69, 1994.

Marshak, A., A. Davis, W. Wiscombe, and G Titov, The verisimilitude of the independent pixel approximation used in cloud remote sensing, *Remote Sens. Environ.*, *52*, 71-78, 1995a.

Marshak, A., A. Davis, W. Wiscombe, and R. Cahalan, Radiative smoothing in fractal clouds, *J. Geophys. Res.*, *100*, 26,247-26,261, 1995b.

Marshak, A., A. Davis, R. Cahalan, and W. Wiscombe, Nonlocal independent pixel approximation, Direct and inverse problems, *IEEE. Trans. Geosci. Remote Sens.*, *36*, 192-205, 1998.

McKee T. B., and S. B. Cox, Scattering of visible radiation by finite clouds, *J. Atmos. Sci*, *31*, 1885-1892, 1974.

Monin, A. S. and A. M. Yaglom, *Statistical Fluid Mechanics: Mechanics of Turbulence*, vol. 2, 874 pp., MIT Press, Cambridge, Mass., 1975.

Nakajima, T., and M. King, Cloud optical parameters as derived from multispectral cloud radiometer, *Proceedings of the FIRE science team workshop*, Vail, Colorado, 321-326, 1988.

Nakajima, T., and M. King, Determination of the optical thickness and effective particle radius of clouds from reflected solar measurements, part I, Theory, *J. Atmos. Sci.*, *47*, 1878-1893, 1990.

Oreopoulos, L., and H. W. Barker, Accounting for subgrid-scale cloud variability in a multi-layer 1D solar radiative transfer algorithm, *Q. J. R. Meteorol. Soc.*, *125*, 301-330, 1999.

Oreopoulos L., and R. Davies, Plane parallel albedo biases from satellite observation, part I, Dependence on resolution and other factors, *J. Clim.*, *11*, 919-932, 1998a.

Oreopoulos L., and R. Davies, Plane parallel albedo biases from satellite observation, part II, Parameterizations for bias removal, *J. Clim.*, *11*,933-944, 1998b.

Schertzer, D., and S. Lovejoy, Scaling non-linear variability in geophysics: Multiple singularities, observables, universality classes, in *Non-linear-Variability in Geophysics, Scaling and Fractals*, edited by D. Schertzer and S. Lovejoy,318 pp., Kluwer, Acad., Norwell, Mass., 1991.

Schmetz, J., On the parameterization of the radiative properties of broken clouds, *Tellus*, *36*, 417-432, 1984.

Szczap, F., H. Isaka, and M. Saute, Inhomogeneity effects of 1D and 2D bounded cascade model clouds on their effective radiative properties, *Phys. and Chem. Earth*, *25*, 83-89, 2000.

Szczap, F., H. Isaka, M. Saute, B. Guillemet, and A. Ioltukhovski, Effective radiative properties of bounded cascade absorbing clouds: Definition of an effective single-scattering albedo, *J. Geophys. Res.*, this issue.

Titov, G. A., Radiative horizontal transport and absorption in stratocumulus clouds, *J. Atmos. Sci.*, *55*, 2549-2560, 1998.

Twomey, S., and T. Cocks, Remotely sensing of cloud parameters from spectral reflectance in the near-infrared, *Contrib. Atmos. Phys.*, *62*, 172-179, 1989.

Wetzel, M. A., and T. H. Vonder Haar, Theoretical development and sensitivity tests of stratus cloud droplet size retrieval method for AVHRR-K/UM, *Remote Sens. Environ.*, *36*, 105-119, 1991.

Zuev, V. E., and G. A.Titov, Radiative transfer in cloud fields with random geometry, *J. Atmos. Sci.*, *52*, 176-190, 1995.

B. Guillemet, H. Isaka, M. Saute, F. Szczap, Laboratoire de Météorologie Physique, Université Blaise Pascal, 24 Avenue des Landais, 63177 Aubière Cedex, France.(e-mail:szczap@opgc.univ-bpclermont.fr)

A. Ioltukhovski, Keldish Institute of Applied Mathematics, 4 Miusskaya Pl. 125047 Moscow, Russia.

(Received March 19, 1999; revised November 8, 1999; accepted January 21, 2000.)